Inverse distribution of hot electrons in a two-level quantum well with nonsymmetric scattering

A. Hernández-Cabrera* and P. Aceituno
Departamento de Física Básica, Universidad de La Laguna, La Laguna, 38206-Tenerife, Spain

F. T. Vasko†
NMRC, University College Cork, Lee Maltings, Prospect Row, Cork, Ireland
and Institute of Semiconductor Physics, NAS Ukraine, Prospekt Nauki 45, Kiev 03650, Ukraine
(Received 15 August 2002; published 9 January 2003)

We have studied the nonequilibrium distribution of electrons accelerated by an in-plane electric field in a stepped quantum well with two closely spaced levels. The spontaneous emission of optical phonons provides an effective cutoff of the electron distribution in the low-temperature case. Taking into account the quasielastic scattering with acoustic phonons (both for intra- and intersubband) and an effective elastic scattering in the second subband, we have found the conditions for the intersubband population inversion of electrons. Next, we have considered the resonant response of a multiquantum well structure placed at the center of a waveguide and found the conditions for the stimulated emission of the THz radiation.

DOI: 10.1103/PhysRevB.67.045304 PACS number(s): 73.50.Bk, 78.66.Fd

I. INTRODUCTION

The distribution of the quasi-two-dimensional (2D) hot electrons in metal-oxide semiconductor (MOS) structures and in selectively doped heterostructures was examined 20 years ago in connection with the realization of the field-effect transistors (see Ref. 1 for a review). The results appeared to be dependent both on the intersubband and on the electron-electron scattering mechanisms. Such mechanisms were taken into account in the framework of the balance equations approach and under the numerical simulation based on the Monte Carlo method. Using these techniques the interlevel redistribution of hot electrons was examined in Ref. 2. The heterostructures with only two closely spaced levels, such as the stepped quantum well (SQW), have been the subject of the investigation by both optical and transport methods during the past decade (see Refs. 3 and 4, respectively). The conditions for the interlevel population inversion due to the heating caused by a longitudinal electric field are considered here.

In this paper we consider the hot electron distribution in a two-level SQW with a strong elastic scattering in the upper subband, which results from the rough external heteroboundaries or from the doped regions near these boundaries [see Fig. 1(a)], subjected to an in-plane electric field. We examine the low-temperature case when electrons are distributed over the passive region (when the energy is smaller than the optical phonon energy $\hbar\omega_{LO}$) due to an effective emission of longitudinal optical (LO) phonons [Fig. 1(b)]. The character of the hot electron distribution in the system considered here is determined both by the peculiarities of the scattering in the passive region (where the momentum relaxation in the second subband is supposed strong enough to make effective the heating of electrons only in the first subband), and by the nonsymmetry of the relaxation rates due to the optical-phonon emission. Taking into account both the intra- and intersubband quasielastic scattering in the passive region, we have found the conditions for the intersubband population inversion and their dependence on the electric field. Further, we use the obtained nonequilibrium distribution in order to consider the dependency of the resonant intersubband response on the transverse field $E_\perp \exp(-i\omega t)$. The propagation of the transverse mode along the THz waveguide, with the multi-SQW structure placed at its center, is also considered. Finally, we discuss the conditions for the stimulated emission regime.

The present work is connected with the current efforts done for the realization of the THz lasing effect based on the intersubband transitions[1–6] caused by the successful application of the cascade structures for the midinfrared (IR) lasing.[7] The stimulated emission regime in tunnel-coupled structures under the vertical transport pump have been lastly reported this year,[8] after the previous investigations of the spontaneous THz emission.[9,10] Thus the study of the conditions for the realization of the inversion population in the structures with closely spaced levels under the longitudinal

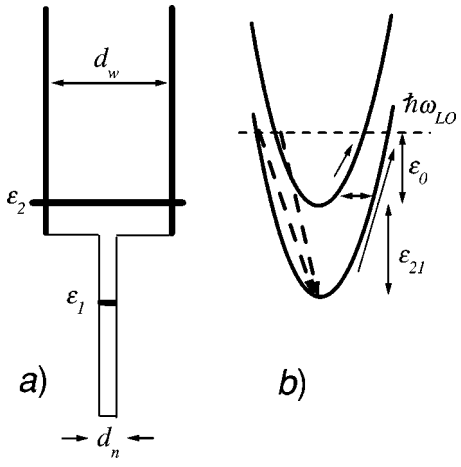

FIG. 1. Energy band diagram of stepped QW with rough external heteroboundaries (or with doped regions near these boundaries) (a) and the dispersion laws of two closely spaced levels (b); solid arrows denote the acceleration due to the electric field, horizontal arrow shows intersubband transitions, and dashed arrows denote spontaneous emission of the optical phonons.

current pumping, among other mechanisms, is of great interest.

This paper is divided into three sections. In Sec. II we evaluate the system of the kinetic equations for the passive region, which governs the hot electron distribution over the two subbands in the SQW under analysis. The solution of this system is performed in Sec. III. The intersubband response of electrons, including the conditions for the stimulated emission regime, is discussed in Sec. IV. Concluding remarks and the list of assumptions made are presented in the last section. The Appendix contains the estimations of the parameters used for the SQW with very different widths.

II. EQUATIONS FOR THE TWO-LEVEL QW

The general system of kinetic equations for the distribution functions of the jth subband, $f_{j\mathbf{p}}$, for the two-level SQW ($j=1,2$) subjected to an in-plane electric field $\mathbf{E}$, is written as follows

$$e\mathbf{E}\cdot\frac{\partial f_{1\mathbf{p}}}{\partial \mathbf{p}} = I_{ac}(f|1\mathbf{p}) + I_{LO}(f|1\mathbf{p}),$$

$$e\mathbf{E}\cdot\frac{\partial f_{2\mathbf{p}}}{\partial \mathbf{p}} = I_{im}(f|2\mathbf{p}) + I_{ac}(f|2\mathbf{p}) + I_{LO}(f|2\mathbf{p}), \qquad (1)$$

where $I_{ac}(f|j\mathbf{p})$ and $I_{LO}(f|j\mathbf{p})$ stand for the collision integrals with acoustic and optical phonons, respectively. $I_{im}(f|2\mathbf{p})$ describes the elastic scattering in the second subband due to the imperfections (roughness of heteroboundaries or donors) placed outside of the narrow well (see Fig. 1). Below we evaluate the collision integrals for the SQW under study and we reduce the system (1) to the equations for the quasi-isotropic distribution functions over the passive region.

A. Collision integrals

It is convenient to divide the acoustic-phonon collision integral from Eqs. (1) into intra- and intersubband contributions,

$$I_{ac}(f|j\mathbf{p}) = \overline{I}_{ac}(f_j|\mathbf{p}) + \tilde{I}_{ac}(f|j\mathbf{p}). \qquad (2)$$

Here $\overline{I}_{ac}(f_j|\mathbf{p})$ describes the momentum and energy relaxation in the jth subband ($j=1,2$)

$$\overline{I}_{ac}(f_j|\mathbf{p}) = \sum_{\mathbf{p}'} (W^{(j)}_{\mathbf{pp}'} f_{j\mathbf{p}'} - W^{(j)}_{\mathbf{p}'\mathbf{p}} f_{j\mathbf{p}}), \qquad (3)$$

and the transition probability

$$W^{(j)}_{\mathbf{pp}'} = \frac{2\pi}{\hbar}\sum_q |C_Q|^2 |\langle j|e^{-iqz}|j\rangle|^2 \times [(2N_Q+1) \times \delta(\varepsilon_p - \varepsilon_{p'} - \hbar\omega_Q) + N_Q \delta(\varepsilon_p - \varepsilon_{p'} + \hbar\omega_Q)] \qquad (4)$$

satisfies the condition $W^{(j)}_{\mathbf{p}'\mathbf{p}} = \exp[(\varepsilon-\varepsilon')/T] W^{(j)}_{\mathbf{pp}'}$ with the phonon temperature T and $j=1,2$ (from now on we will use T instead of k_BT, and T means thermal energy). The intersubband collision integrals in Eq. (2) are given by

$$\tilde{I}_{ac}(f|1\mathbf{p}) = \sum_{\mathbf{p}'} W^{(12)}_{\mathbf{pp}'}(f_{2\mathbf{p}'} - f_{1\mathbf{p}}), \quad \tilde{I}_{ac}(f|2\mathbf{p}) = \sum_{\mathbf{p}'} W^{(21)}_{\mathbf{pp}'}(f_{1\mathbf{p}'} - f_{2\mathbf{p}}) \qquad (5)$$

with the transition probabilities ($j \neq j'$)

$$W^{(jj')}_{\mathbf{pp}'} \simeq \frac{2\pi}{\hbar}\sum_q |C_Q|^2 |\langle j|e^{-iqz}|j'\rangle|^2 (2N_Q+1)\,\delta(\varepsilon_{jj'} + \varepsilon_p - \varepsilon_{p'}), \qquad (6)$$

which are written for the elastic approximation. The electron dispersion laws ε_{jp} are given by $\varepsilon_j + \varepsilon_p$, where $\varepsilon_p = p^2/2m$, with m the effective mass, and $\varepsilon_{jj'} = \varepsilon_j - \varepsilon_{j'}$ is the interlevel splitting energy. The above transition probabilities are expressed through the bulk matrix element for the deformation electron-phonon interaction C_Q. Finally, N_Q is the Plank distribution of the acoustic phonons with frequency $\omega_Q = sQ$; here $\mathbf{Q} \equiv [(\mathbf{p}-\mathbf{p}')/\hbar, q]$ is the three-dimensional (3D) phonon wave vector and s is the velocity of sound. For the low-temperature case ($\hbar\omega_{LO} \gg T$) and only taking into account the spontaneous emission, the collision integral for LO phonons in the system (1) is written as:

$$I_{LO}(f|j\mathbf{p}) = \frac{2\pi}{\hbar}\sum_{j'\mathbf{Q}} \left| C_Q^{(LO)}\right|^2 |\langle j|e^{-iqz}|j'\rangle|^2 \times [\,\delta(\varepsilon_{jp} - \varepsilon_{j'\mathbf{p}+\hbar\mathbf{q}} + \hbar\omega_{LO}) f_{j'\mathbf{p}+\hbar\mathbf{q}} - \delta(\varepsilon_{jp} - \varepsilon_{j'\mathbf{p}-\hbar\mathbf{q}} - \hbar\omega_{LO}) f_{j\mathbf{p}}], \qquad (7)$$

where ω_{LO} is the dispersionless LO-phonon frequency and $C_Q^{(LO)}$ is the bulk matrix element for the Frölich interaction.

From now on we will consider a quasi-isotropic distribution for the case of strong momentum relaxation in the second subband if $\nu_{im} \gg \nu_{ac}$ and $eE/\nu_{im} \ll \overline{p}$; here $\overline{p}$ is the typical 2D momentum, ν_{im} and ν_{ac} are the characteristic momentum relaxation rates (the explicit form of the elastic collision integral in the second subband is only necessary when the above inequalities are not accomplished and we do not present it here). Under the above conditions one can neglect anisotropic contributions in the second subband and take into account the weak (of the order of $eE/\nu_{ac}\overline{p} \ll 1$) anisotropic correction to the distribution in the first subband. Thus we search the solution of Eqs. (1) in the form

$$f_{1\mathbf{p}} \simeq f_{1\varepsilon} + \Delta f_{1\mathbf{p}}, \quad f_{2\mathbf{p}} \simeq f_{2\varepsilon}. \qquad (8)$$

Separating the asymmetric part of the equation for $f_{1\mathbf{p}}$ in the system (1) and using the elastic approximation in the collision integral of Eq. (3) with the condition $\hbar\omega_Q \gg T$ we obtain $\Delta f_{1\mathbf{p}}$ as follows:

$$\Delta f_{1\mathbf{p}} \simeq -\frac{e}{m}(\mathbf{E}\cdot\mathbf{p})\frac{df_{1\varepsilon}}{d\varepsilon}\nu_{1\varepsilon}^{-1},$$

$$\nu_{1\varepsilon}=\frac{\pi D^2 T\rho_{2D}}{\hbar s^2\rho}[K_{11}+K_{12}\theta(\varepsilon-\varepsilon_{21})]. \tag{9}$$

Here D is the deformation potential, ρ is the crystal density and ρ_{2D} is the 2D density of states. The relaxation frequency $\nu_{1\varepsilon}$ is obtained as the sum of the intra- and intersubband contributions, which are determined by the characteristic wave vectors:

$$K_{jj'}=\int_{-\infty}^{\infty}\frac{dq}{2\pi}|\langle j|e^{-iqz}|j'\rangle|^2=\int dz\,\phi_j^2(z)\phi_{j'}^2(z), \tag{10}$$

where $\phi_j(z)$ is the orbital of jth subband.

The system of equations for the symmetric distribution functions $f_{j\varepsilon}$ is obtained after averaging Eqs. (1) over the **p**-plane angle φ. The field dependent contribution is absent in the equation for $f_{2\varepsilon}$. The left side of the equation for $f_{1\varepsilon}$ is written as $\int_0^{2\pi}(d\varphi/2\pi)e\mathbf{E}\cdot\partial\Delta f_{1\mathbf{p}}/\partial\mathbf{p}$. Using the standard quasielastic approximation for the isotropic parts of the collision integrals $\int_0^{2\pi}(d\varphi/2\pi)\overline{I}_{ac}(f_j|\mathbf{p})$ and taking into account the energy conservation laws in the LO-phonon collision integrals we obtain the system of equations corresponding to the symmetric distribution functions in the form

$$\frac{dJ_1(\varepsilon)}{d\varepsilon}+\tilde{\nu}\theta(\varepsilon-\varepsilon_{21})(f_{2\varepsilon-\varepsilon_{21}}-f_{1\varepsilon})$$
$$+\sum_j[\nu_{1j}^{+}(\varepsilon)f_{j\varepsilon+\varepsilon_{1j}+\hbar\omega_{LO}}-\nu_{1j}^{-}(\varepsilon)f_{1\varepsilon}]=0,$$
$$\frac{dJ_2(\varepsilon)}{d\varepsilon}+\tilde{\nu}(f_{1\varepsilon+\varepsilon_{21}}-f_{2\varepsilon})$$
$$+\sum_j[\nu_{2j}^{+}(\varepsilon)f_{j\varepsilon+\varepsilon_{2j}+\hbar\omega_{LO}}-\nu_{2j}^{-}(\varepsilon)f_{2\varepsilon}]=0. \tag{11}$$

The LO-phonon frequencies are introduced in Eq. (11) according to

$$\nu_{jj'}^{\pm}(\varepsilon)=\frac{2\pi}{\hbar}\sum_{j'\mathbf{p}'}|C_Q^{(LO)}|^2|\langle j|e^{-iqz}|j'\rangle|^2\delta(\varepsilon-\varepsilon_{p'}\pm\hbar\omega_{LO}) \tag{12}$$

and the energy fluxes over the first and second subbands are given by

$$J_1(\varepsilon)=\frac{(eE)^2\varepsilon}{m\nu_{1\varepsilon}}\frac{df_{1\varepsilon}}{d\varepsilon}+\nu_1(2ms^2\varepsilon+E_1^2)\left(\frac{df_{1\varepsilon}}{d\varepsilon}+\frac{f_{1\varepsilon}}{T}\right),$$
$$J_2(\varepsilon)=\nu_2(2ms^2\varepsilon+E_2^2)\left(\frac{df_{2\varepsilon}}{d\varepsilon}+\frac{f_{2\varepsilon}}{T}\right). \tag{13}$$

The inter- and intrasubband relaxation frequencies in Eqs. (11) and (13), $\tilde{\nu}$ and ν_j, respectively, are determined as follows:

$$\tilde{\nu}=\frac{\pi D^2 T\rho_{2D}}{\hbar s^2\rho}K_{12},\quad \nu_j=\frac{\pi D^2 T\rho_{2D}}{\hbar s^2\rho}K_{jj}. \tag{14}$$

The characteristic energy values $E_{1,2}$ are introduced through the relations

$$K_{jj}E_j^2=\int_{-\infty}^{\infty}\frac{dq}{4\pi}(\hbar sq)^2|\langle j|e^{-iqz}|j\rangle|^2$$
$$=\frac{(\hbar s)^2}{2}\int dz\left(\frac{d\phi_j^2(z)}{dz}\right)^2. \tag{15}$$

The system of the second-order equations (11) with the fluxes of Eqs. (13) should be solved with the standard boundary conditions

$$f_{j\varepsilon\to\infty}=0,\quad J_1(\varepsilon\to 0)=0, \tag{16}$$

and with the normalization condition

$$\rho_{2D}\sum_j\int_0^{\infty}d\varepsilon f_{j\varepsilon}=n_{2D}, \tag{17}$$

where n_{2D} is the concentration of 2D electrons and ρ_{2D} is the density of states. The condition for the energy flux at $\varepsilon\to 0$ corresponds to the absence of capture processes for slow electrons.

B. Boundary conditions

If the LO-phonon emission is the most effective process, the electron distribution rapidly decreases in the active region, where the energy is bigger than $\hbar\omega_{LO}$. Therefore the incoming contributions to the last term of Eq. (10) are absent in the active region as well as there are no outgoing contributions from the second subband because $\overline{\nu}_{12}(\varepsilon=\hbar\omega_{LO})=0$ and $\overline{\nu}_{22}(\varepsilon=\hbar\omega_{LO}-\varepsilon_{21})=0$. As a result, the system (11) is transformed in the active region as follows

$$\frac{dJ_1(\varepsilon)}{d\varepsilon}+\tilde{\nu}\theta(\varepsilon-\varepsilon_{21})(f_{2\varepsilon-\varepsilon_{21}}-f_{l\varepsilon})-\overline{\nu}_{11}(\varepsilon)f_{1\varepsilon}=0,$$
$$\varepsilon>\hbar\omega_{LO},$$
$$\frac{dJ_2(\varepsilon)}{d\varepsilon}+\tilde{\nu}(f_{1\varepsilon+\varepsilon_{21}}-f_{2\varepsilon})-\overline{\nu}_{21}(\varepsilon)f_{2\varepsilon}=0,$$
$$\varepsilon>\hbar\omega_{LO}-\varepsilon_{21}. \tag{18}$$

In the passive region (where the energy is smaller than $\hbar\omega_{LO}$) there are not outgoing processes and the system (11) takes the form

$$\frac{dJ_1(\varepsilon)}{d\varepsilon}+\tilde{\nu}\theta(\varepsilon-\varepsilon_{21})(f_{2\varepsilon-\varepsilon_{21}}-f_{l\varepsilon})$$

$$+\sum_j \nu_{1j}^{+}(\varepsilon)f_{j\varepsilon+\varepsilon_{1j}+\hbar\omega_{LO}}=0, \quad \varepsilon<\hbar\omega_{LO},$$

$$\frac{dJ_2(\varepsilon)}{d\varepsilon}+\tilde{\nu}(f_{1\varepsilon+\varepsilon_{21}}-f_{2\varepsilon})=0, \quad \varepsilon<\hbar\omega_{LO}-\varepsilon_{21}. \quad (19)$$

These systems are connected by the additional four boundary conditions:

$$f_{j\varepsilon}|_{\varepsilon_j-0}^{\varepsilon_j+0}=0, \quad J_j(\varepsilon)|_{\varepsilon_j-0}^{\varepsilon_j+0}=0,$$

$$\varepsilon_j=\begin{cases}\hbar\omega_{LO}, & j=1\\ \hbar\omega_{LO}-\varepsilon_{21}, & j=2\end{cases}, \quad (20)$$

where ε_j stand for the boundary energy values between passive and active regions.

Under the inequalities $\overline{\nu}_{11}(\hbar\omega_{LO})/\nu_1 \gg 1$ and $\overline{\nu}_{21}(\varepsilon_2)/\nu_2 \gg 1$, the distributions $f_{j\varepsilon}$ quickly fall in the active region and one can consider simplified independent equations instead of the system (18):

$$\frac{d^2f_{j\varepsilon}}{d\varepsilon^2}-\lambda_j^2 f_{j\varepsilon}=0, \quad \varepsilon>\varepsilon_j \quad (21)$$

with the characteristic decreasing factors

$$\lambda_1=\sqrt{\frac{\overline{\nu}_{11}(\hbar\omega_{LO})/\nu_1}{(\varepsilon_f+2ms^2)\hbar\omega_{LO}+E_1^2}}, \quad \lambda_2=\sqrt{\frac{\overline{\nu}_{21}(\varepsilon_2)/\nu_2}{2ms^2\varepsilon_2+E_1^2}}. \quad (22)$$

Here we have introduced the characteristic field-dependent energy $\varepsilon_f=(eE/\nu_1)^2/[m(1+K_{12}/K_{11})]$. The solutions for the active region take the forms

$$f_{j\varepsilon}\simeq f_{j\varepsilon=\varepsilon_j-0}e^{-\lambda_j(\varepsilon-\varepsilon_j)}, \quad (23)$$

where we have used the boundary conditions of Eq. (20) for $f_{1,2\varepsilon}$. With these solutions the boundary conditions for energy fluxes of Eq. (19) are transformed into

$$\left.\frac{df_{j\varepsilon}}{d\varepsilon}\right|_{\varepsilon_j}+\lambda_j f_{j\varepsilon=\varepsilon_j}=0. \quad (24)$$

Thus we have solved the system (19) over the passive region by using only the boundary conditions of Eq. (24), the additional condition for $J_1(\varepsilon)$ from Eq. (16) and the normalization condition of Eq. (17). The incoming contribution to the first Eq. (19) is written using Eq. (23) in the form

$$+\sum_j \nu_{1j}^{+}(0)f_{j\varepsilon_j}e^{-\lambda_j\varepsilon}. \quad (25)$$

This contribution quickly falls near $\varepsilon=0$. So that, it is convenient to use a new boundary condition at small energy $\overline{\varepsilon}$, which is of the order of λ_j^{-1}. The integration of the first equation of the system (19) over the region $(0,\overline{\varepsilon})$ gives us the new boundary condition at small energy in the form

$$J_1(\varepsilon\to 0)+\sum_j \nu_{1j}^{+}(0)\frac{f_{1\varepsilon_j}}{\lambda_j}=0. \quad (26)$$

This condition corresponds to the conservation of the total-energy flux over the passive region.

III. HIGH-FIELD DISTRIBUTION FUNCTION

Let us turn back to consider the hot electron distribution in the passive region. For reasons of convenience, we will split the distribution function in the first subband into two functions: $f_\varepsilon^<=f_{1\varepsilon}$, if $\varepsilon<\varepsilon_{21}$, and $f_\varepsilon^>=f_{1\varepsilon-\varepsilon_{21}}$, if $\varepsilon>\varepsilon_{21}$. Thus the system (18) is transformed into a separate equation for $f_\varepsilon^<$:

$$\frac{d}{d\varepsilon}\left\{[(\varepsilon_f+2ms^2)\varepsilon+E_1^2]\frac{df_\varepsilon^<}{d\varepsilon}+\frac{2ms^2\varepsilon+E_1^2}{T}f_\varepsilon^<\right\}=0,$$

$$\varepsilon<\varepsilon_{21} \quad (27)$$

and two coupled equations for $f_\varepsilon^<$ and $f_{2\varepsilon}$ over the interval $0<\varepsilon<\varepsilon_2$:

$$\frac{dJ^>(\varepsilon)}{d\varepsilon}+k_1(f_{2\varepsilon}-f_\varepsilon^>)=0,$$

$$\frac{dj_2(\varepsilon)}{d\varepsilon}+k_2(f_\varepsilon^>-f_{2\varepsilon})=0. \quad (28)$$

Here we have introduced the dimensionless parameters $k_j=K_{12}/K_{jj}$, which describe the efficiency of the intersubband transitions caused by the elastic scattering. The energy flux $J^>(\varepsilon)$ in Eq. (28) is given by

$$J^>(\varepsilon)=[(\varepsilon_f+2ms^2)(\varepsilon+\varepsilon_{21})+E_1^2]$$
$$\times\frac{df_\varepsilon^>}{d\varepsilon}+\frac{2ms^2(\varepsilon+\varepsilon_{21})+E_1^2}{T}f_\varepsilon^>, \quad (29)$$

while $j_2(\varepsilon)=J_2(\varepsilon)/\nu_2$ is determined by Eq. (13). Simultaneously with such separation of equations for $f_{1\varepsilon}$ we have to include the additional boundary conditions: $f_{\varepsilon=\varepsilon_{21}}^<=f_{\varepsilon=0}^>$ and $J_1(\varepsilon)|_{\varepsilon_{21}-0}^{\varepsilon_{21}+0}=0$.

Using the condition for the conservation of the energy flux in Eq. (26) we transform Eq. (27) into the nonuniform first-order equation:

$$[(\varepsilon_f+2ms^2)\varepsilon+E_1^2]\frac{df_\varepsilon^<}{d\varepsilon}+\frac{2ms^2\varepsilon+E_1^2}{T}f_\varepsilon^<$$
$$=-\sum_j \nu_{1j}^{+}(0)\frac{f_{1\varepsilon_j}}{\nu_1\lambda_j}, \quad (30)$$

which can be integrated exactly. The function $f_\varepsilon^<$ takes the form

TABLE I. Parameters used in calculations for the three samples studied in the text.

	ε_2 (meV)	d_w (Å)	d_n (Å)	k_1	k_2	E_2 (meV)	λ_2^{-1} (meV)	ν_{12}^+/ν_1
(a)	10	414.0	21.5	0.40	0.77	0.58	0.64	2.50
(b)	18	498.0	18.0	0.23	0.53	0.48	0.73	1.83
(c)	24	610.0	14.6	0.12	0.36	0.39	0.84	1.22

$$f_\varepsilon^< = e^{-\Theta_\varepsilon}\left[N - \sum_j \nu_{1j}^+(0)\frac{f_{1\varepsilon_j}}{\nu_1\lambda_j}\int \frac{d\varepsilon\,\exp(\Theta_\varepsilon)}{(\varepsilon_f+2ms^2)\varepsilon+E_1^2}\right],$$

$$\Theta_\varepsilon = \int \frac{d\varepsilon}{T}\frac{2ms^2\varepsilon+E_1^2}{(\varepsilon_f+2ms^2)\varepsilon+E_1^2}, \tag{31}$$

where N is the normalization constant determined from the condition of Eq. (17). Further simplification is possible for the strong electric field case, $\varepsilon_f \gg 2\ \mathrm{ms}^2$. As a result, the four boundary conditions for $f_\varepsilon^<$ and $f_\varepsilon^>$ transforms into

$$\left.\frac{df_\varepsilon^>}{d\varepsilon}\right|_{\varepsilon_2} + \lambda_1 f^>_{\varepsilon=\varepsilon_2} = 0, \quad \left.\frac{df_{2\varepsilon}}{d\varepsilon}\right|_{\varepsilon_2} + \lambda_2 f_{2\varepsilon=\varepsilon_2} = 0,$$

$$f^>_{\varepsilon=0} = f^<_{\varepsilon=\varepsilon_{21}}, \quad \frac{\varepsilon_f\varepsilon_{21}/(1+k_1)+E_1^2}{\varepsilon_f\varepsilon_{21}+E_1^2}\left.\frac{df_\varepsilon^>}{d\varepsilon}\right|_{\varepsilon=0} = \left.\frac{df_\varepsilon^<}{d\varepsilon}\right|_{\varepsilon_{21}}. \tag{32}$$

Thus we must solve the system of two second-order equations (28), valid for the interval $(0,\varepsilon_2)$, together with the boundary conditions of Eq. (32).[11]

The numerical solution of the formulated problem is obtained in the framework of the Burlirsch-Stoer method[12] for systems including functions without known initial values as $f_{2\varepsilon}$ is. The calculations are performed here for a $Al_{0.14}Ga_{0.86}As/GaAs/Al_{0.14}Ga_{0.86}As$ SQW's with the parameters presented in Table I. For the three cases under study $E_1 = 0.92$ meV, $\nu_{11}^+/\nu_1 = 14.79$, and λ^{-1} varies from 0.64 meV ($\varepsilon_f = 1$ meV) to 8.55 meV ($\varepsilon_f = 30$ meV). These parameters have been estimated in the basis of the simplified consideration included in the Appendix. The different cases correspond to the interlevel energy values $\varepsilon_{21} = 26$ meV (a), 18 meV (b), and 12 meV (c). In Fig. 2 we illustrate the evolution of the distribution functions $f_{1,2\varepsilon}$ starting from the Boltzmann distribution (which is shown here and below by the short-dashed curves) to the nonequilibrium distributions over the passive region. Curves have been obtained for the helium temperature case, $T = 4.2$ K, and for three different electric fields. Figures 3(a)–(c) show the evolution of $f_{1,2\varepsilon}$ with the further increase of ε_f. Note that $\varepsilon_f = 10$ meV corresponds to the field strengths of 3.6 V/cm (a), 5.1 V/cm (b), and 12.8 V/cm (c), respectively. One can see that electrons become distributed over the all passive region if $\varepsilon_f > 18.5$ meV (a), $\varepsilon_f > 23$ meV (b), and $\varepsilon_f > 16.5$ meV (c), respectively, and the interwell redistribution appears mainly due to the spontaneous emission of the optical phonons. The interlevel redistribution increases with ε_f and the same level of redistribution occurs for different ε_{21} if ε_f is the same [compare the cases (a)–(c)]. The tails of the distribution in the active region remain as a weak contribution (less than 15% of the total concentration) up to $\varepsilon_f \simeq 30$ meV.

If the temperature increases, one needs a higher electric field for the realization of the interlevel redistribution. This is illustrated in Fig. 4 where we plot the distribution functions for the case (b) at $T = 20$ K. Since we consider the nondegenerate electron case, the presented distributions are simply proportional to 2D concentration through the normalization condition of Eq. (17). Thus we use here the Y scale normalized to the zero-energy value of the Boltzmann function $f_B(\varepsilon_f = 0\ \mathrm{meV})$.

IV. INTERSUBBAND RESPONSE

In this section we consider the resonant response of the hot electrons subjected to a weak transverse electric field $E_\perp \exp(-i\omega t)$ and describe the negative absorption due to the inverse population of the subbands. We also consider an unstable mode in the THz waveguide with the multi-SQW's placed at its center in order to estimate the characteristic length of the instability which determines the possibility of the stimulated emission regime.

A. Resonant transitions

Using the resonant approximation, we write the induced high-frequency current δI_ω as $\delta I_\omega \simeq (2e/L^2)\Sigma_{\mathbf{p}} v_\perp \delta f_{21\mathbf{p}}$ where $v_\perp = \langle 1|\hat{v}_z|2\rangle$ is the transverse velocity matrix element and L^2 is the normalization area. The resonant addendum to the density matrix, $\delta f_{21\mathbf{p}} \exp(-i\omega t)$, is determined from the linearized kinetic equation:

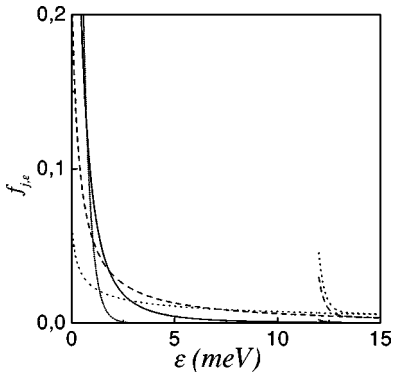

FIG. 2. Distribution functions $f_{j,\varepsilon}$ for low electric fields ($\varepsilon_f \leqslant 5$ meV) compared with the Boltzmann function ($\varepsilon_f = 0$ meV, short-dashed line). Solid line: $\varepsilon_f = 1$ meV. Dashed line: $\varepsilon_f = 2.5$ meV. Dotted line: $\varepsilon_f = 5$ meV.

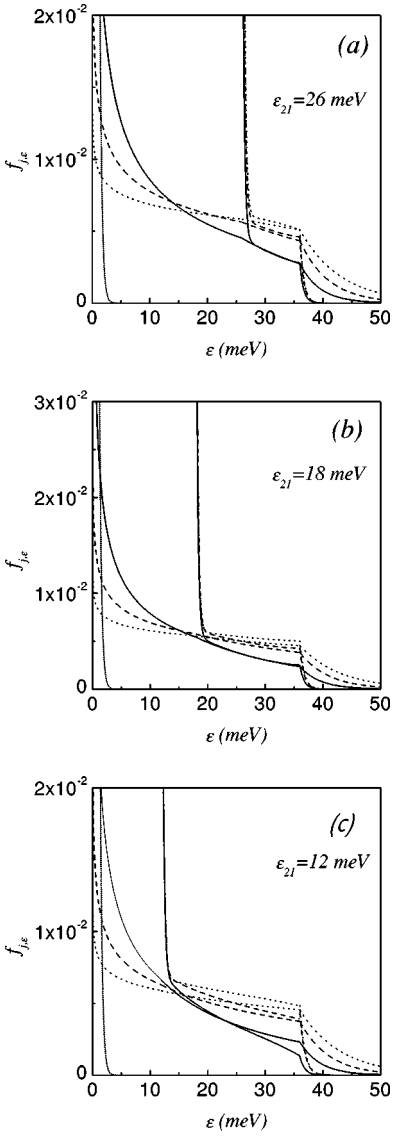

FIG. 3. Evolution of $f_{j,\varepsilon}$ with the increase of ε_f: $\varepsilon_f=5$ meV (solid curves), $\varepsilon_f=10$ meV (dashed curves), and $\varepsilon_f=20$ meV (dotted curves) for the SQW's (a)–(c) (see parameters in the table).

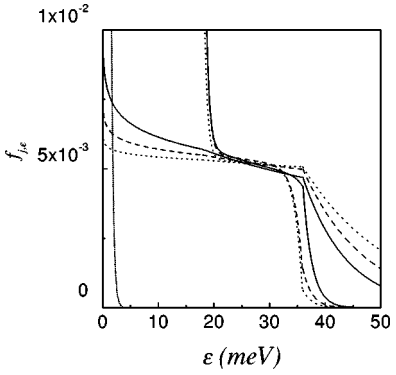

FIG. 4. The same as in Fig. 3 for the SQW's [case (b)] at $T=20$ K.

$$(-i\omega+e\mathbf{E}\cdot\nabla_p)\delta f_{21\mathbf{p}}+\frac{i\varepsilon_{21}}{\hbar}\delta f_{21\mathbf{p}}+\frac{i}{\hbar}\delta h_{21}(f_{1\mathbf{p}}-f_{2\mathbf{p}})$$
$$=J_{21}(\delta f|\mathbf{p}), \tag{33}$$

with the perturbation operator $\delta h_{21}=(ie/\omega)E_\perp v_\perp$, and the linearized collision integral $J_{21}(\delta f|\mathbf{p})$. Supposing here $eE/\omega\ll\overline{p}$ and $eE/\nu\ll\overline{p}$, we can neglect both $e\mathbf{E}\cdot\nabla_p$ and the nonsymmetric contributions to the steady-state distribution functions $f_{1,2\mathbf{p}}$. Also, replacing the collision integral by $-\gamma_\varepsilon\delta f_{21\mathbf{p}}/\hbar$, γ_ε being the effective broadening energy of the resonant peak, we write the equation for $\delta f_{21\mathbf{p}}\simeq\delta f_{21}(\varepsilon)$ in the form

$$(\hbar\omega-\varepsilon_{21}+i\gamma_\varepsilon)\delta f_{21}(\varepsilon)+\frac{ie}{\omega}E_\perp v_\perp(f_{1\varepsilon}-f_{2\varepsilon})=0. \tag{34}$$

Taking into account both the elastic mechanism of broadening and the LO-phonon emission, we approximate γ_ε by a step function $\gamma_\varepsilon\simeq\gamma$ if $\varepsilon<\varepsilon_2$ and $\gamma_\varepsilon=\gamma_{LO}$ if $\varepsilon>\varepsilon_2$.

The induced current is written in the form $\delta I_\omega=\sigma_\omega E_\perp$ and the complex conductivity is given by

$$\sigma_\omega=\frac{e^2|v_\perp|^2}{\omega}\frac{2}{L^2}\sum_{\mathbf{p}}\frac{f_{1\varepsilon}-f_{2\varepsilon}}{\varepsilon_{21}-\hbar\omega-i\gamma_\varepsilon}. \tag{35}$$

Neglecting $\mathrm{Im}(\sigma_\omega)$ for the near-resonant region and using the above-introduced stepped broadening γ_ε we obtain the maximum of $\mathrm{Re}(\sigma_\omega)$, when $\hbar\omega\simeq\varepsilon_{21}$, as follows:

$$\sigma_{\max}=\mathrm{Re}(\sigma_{\omega=\varepsilon_{21}/\hbar})=\frac{e^2|v_\perp|^2\hbar}{\varepsilon_{21}\gamma}$$
$$\times\rho_{2D}\left[\int_0^{\varepsilon_2}d\varepsilon(f_{1\varepsilon}-f_{2\varepsilon})+\frac{\gamma}{\gamma_{LO}}\int_{\varepsilon_2}^{\hbar\omega_{LO}}d\varepsilon f_{1\varepsilon}\right]. \tag{36}$$

Thus the condition for the negative absorption, $\sigma_{\max}<0$, is written as $\int_0^{\varepsilon_2}d\varepsilon(f_{1\varepsilon}-f_{2\varepsilon})<0$, if one can neglect the second addendum in Eq. (36) (the condition $\gamma/\gamma_{LO}\ll1$ is valid for samples without strong inhomogeneous broadening). This condition corresponds to the transition from the intersubband absorption to the spontaneous emission regime.

The relative absorption ξ_ω, which is introduced as the ratio of the absorbed power to the incident power,[13] is expressed through the 2D conductivity of Eq. (35) according to $\xi_\omega=4\pi\,\mathrm{Re}(\sigma_\omega)/(c\sqrt{\epsilon})$, where ϵ is the dielectric permittivity, which is supposed uniform across the structure. The maximal value of the relative absorption appears at the condition $\hbar\omega\simeq\varepsilon_{21}$. In Fig. 5 we plot the maximal absorption ξ_{max} versus ε_f for a ten-layer structure with a 2D concentration $n_{2D}=3\times10^{10}$ cm^{-2} and $\epsilon=12.9$. This figure shows the conditions for the negative absorption regime for the SQW's considered in Sec. III. One can see that the population inversion appears at $\varepsilon_f=18.5$ meV for the case (a), 23 meV (b), and 16.5 meV (c). It should be noted that there is a certain ''symmetry'' of the absorption behavior around the $\varepsilon_{21}=\varepsilon_2$ case. In spite of ξ_{max} is suppressed with the increase of ε_f, the population inversion cannot be realized at $T=20$ K (see dot-dashed curve in Fig. 5).

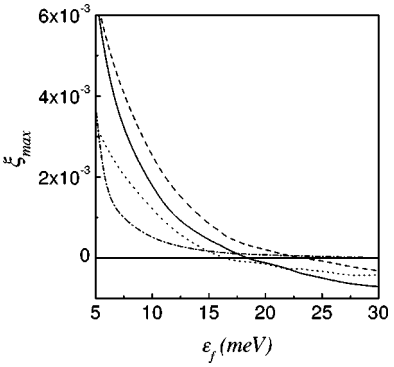

FIG. 5. Maximal value of the relative absorption ξ_{max} vs the characteristic field-dependent energy ε_f for the SQW's at $T=4.2$ K (solid line: $\varepsilon_{21}=26$ meV; dashed line: $\varepsilon_{21}=18$ meV; and dotted line: $\varepsilon_{21}=12$ meV) and for $\varepsilon_{21}=18$ meV at $T=20$ K (dot-dashed line).

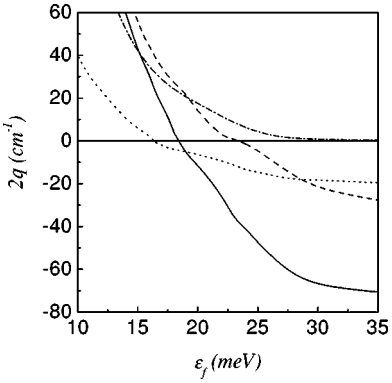

FIG. 6. Maximal modal gain, $g=-2q$ vs ε_f for the SQW's marked as in Fig. 5.

B. Stimulated emission regime

Further we consider propagation of the transverse (polarized along OZ) mode in the resonator of width L. The multi-SQW's structure is placed at the center, around $z=0$, and the ideal mirrors at $z=\pm L/2$ are described by the zero boundary conditions for the wave equation:

$$\left[\Delta+\epsilon\left(\frac{\omega}{c}\right)^2\right]E_{\omega\mathbf{r}}=-i\frac{4\pi\omega}{c^2}I_{\omega\mathbf{r}}. \tag{37}$$

The transverse current is given by $I_{\omega\mathbf{r}}\simeq N\sigma_{\Delta\omega}\delta_N(z)E_{\omega\mathbf{r}}$ with the form-factor $\delta_N(z)$ located in the vicinity of $z=0$. Below we consider the mode propagating along OX and we separate the variables replacing $E_{\mathbf{r}}$ by $E_x\mathcal{E}_z$. The in-plane propagation is described by the equation $(d^2/dx^2+K^2)E_x=0$ while the transverse structure of the mode is determined by:

$$\left(\frac{d^2}{dz^2}+k^2\right)\mathcal{E}_z=-iQ_{\Delta\omega}\delta_N(z)\mathcal{E}_{z=0},\quad k^2=\epsilon\left(\frac{\omega}{c}\right)^2-K^2. \tag{38}$$

The characteristic wave vector $Q_{\Delta\omega}$ is introduced here as follows: $Q_{\Delta\omega}=4\pi\Omega\sigma_{\Delta\omega}N/c^2$.

Supposing that the width of the N-layer structure is much shorter than k^{-1}, we replace the right side of Eq. (38) by the boundary conditions: $\mathcal{E}_z|_{-0}^{0}=0$ and $(d\mathcal{E}_z/dz)|_{-0}^{0}=-iQ_{\Delta\omega}\mathcal{E}_{z=0}$. These conditions, together with the requirement $\mathcal{E}_{z=\pm L/2}=0$, describes the modes formed by the fundamental solutions $\exp(\pm ikz)$ for the intervals $(-L/2,0)$ and $(0,L/2)$. The modes are characterized by the complex wave vectors k_n with $n=1,2\ldots$. Since $Q_{\Delta\omega}L\gg 1$, the even modes do not interact with SQW structure and $k_n\simeq n\pi/L-iQ_{\Delta\omega}/n\pi$ for the odd modes, $n=1,3\ldots$. The propagation along OX is described by the complex wave number $K_n\simeq\tilde{k}_n+iQ_{\Delta\omega}/\tilde{k}_nL$ with $\tilde{k}_n=\pm\sqrt{\epsilon(\Omega/c)^2-(n\pi/L)^2}$. Thus the minimal increment for the lowest mode $n=1$, which corresponds to the field distribution $E_x\propto\exp(-qx)$ or to the mode intensity $\propto\exp(-2qx)$, is determined by

$$q=\frac{Q_{\Delta\omega}}{\tilde{k}_1L}=\frac{4\pi\Omega N\sigma_{\Delta\omega}}{c^2\sqrt{\epsilon(\Omega L/c)^2-\pi^2}}, \tag{39}$$

where the condition $q<0$ corresponds to the unstable mode. We define $g=-2q$ as the gain coefficient for the fundamental mode in the structure under consideration.

For the numerical estimation of the maximal gain we use in Eq. (39) the peak value of the conductivity, at $\Delta\omega=0$. The results for the above discussed cases (a)–(c) are presented in Fig. 6 where we have used $L=6.3$ μm, $L=9.1$ μm, and $L=13.6$ μm [cases (a), (b), and (c), respectively] and considered a ten-layer structure with $n_{2D}=3\times10^{10}$ cm^{-2} for each layer. Since the gain appears to be comparable with the experimental result in Ref. 8 if $\varepsilon_f\geqslant 20$ meV, one can expect the realization of the stimulated emission regime in structures with a few millimeters of lateral size, even if additional losses appears to be visible.

V. CONCLUSION

The nonequilibrium distribution of 2D electrons over the two closely spaced levels with different elastic scattering, under heating by an in-plane electric field, have been obtained for the low-concentration case. Both the intra- and interlevel scattering by acoustic phonons and the spontaneous emission of optical phonons are taken into account in the quasi-isotropic approximation. The conditions for the population inversion have been found and the regime of stimulated THz emission of the mode propagating along the waveguide, with the multi-SQW structure placed at its center, have been described.

Next, we discuss the assumptions used in the present calculations. The main restriction of the results is the consideration of the low-concentration case, neglecting the Coulomb interaction. On one hand, the electron-electron scattering imposes the Maxwell distribution with an effective temperature suppressing the high-energy part of the distribution. On the other hand, an additional channel for the interlevel relaxation due to Auger-like processes damps the interlevel redistribution of electrons. The evaluation of the limiting concentration requires the consideration of more complicate kinetic equations with the electron-electron collision integrals and lies beyond the scope of this paper. In the above presented

numerical estimations we have used a 2D concentration range lower than 10^{11} cm^{-2}, where the electron-electron scattering is not the main scattering process (see Ref. 14, where different systems were considered). In addition, it should be noted that the Coulomb renormalization of the intersubband transition is weak for the concentration region under consideration (see similar estimation of the shift of the intersubband resonance due to redistribution of electrons in Ref. 15).

Another approximation we have made is rather standard. In order to estimate the coefficients of the kinetic equation, we have used in the Appendix a simplified description of the electronic states. It is easy to verify these results performing the straightforward calculations. The use of the bulk model of the phonon dispersion and the electron-phonon interaction is a reasonable approximation for the GaAs/AlGaAs structures.[16] Finally, the phenomenological description of the intersubband transition broadening is a generally accepted approach. It should be also noted that the interlevel redistribution considered in this work suppresses the anisotropic addendum $\Delta f_{1\mathbf{p}}$ given by Eq. (9). Furthermore, due to the effective momentum relaxation in the upper subband, a negative differential conductivity occurs with the increase of ε_f. For the parameters used in Sec. III, a noticeable negative differential conductivity appears for $\varepsilon_f \simeq 3$ meV and current instabilities in time or spacial domains (along the current direction) are possible.[17] But both the conductivity and its field derivative are suppressed with the further increase of ε_f. These phenomena appear not to be essential for $\varepsilon_f > 20$ meV where the stimulated emission regime takes place. In addition, since the current and the mode propagation directions are perpendicular, a sample may be short enough along the current direction to avoid instabilities. A detailed description of unstable response in the high-mobility structures discussed in the present work requires a special consideration.

To conclude, the present analysis shows the possibility of obtaining the inversion of the electron distribution in a stepped QW with nonsymmetric scattering in the low concentration region. Besides the stimulated emission regime in the THz waveguide discussed here, a negative differential resistance can be achieved under the interlevel redistribution of electrons. In addition, the multi-SQW structure may be of great interest for the modulation of the THz radiation. These cases will be considered elsewhere. We expect that the presented results will stimulate the experimental treatment of the considered system.

ACKNOWLEDGMENTS

This work has been supported in part by Consejería de Educación, Cultura y Deportes, Gobierno Autónomo de Canarias, and by the Science Foundation of Ireland.

APPENDIX A: SQW MODEL WITH $d_w \gg d_n$

Here we present the estimations for the parameters of the kinetic equation considered in Sec. II A [the energy $E_{1,2}$, determined by Eq. (15), and the dimensionless coefficients $k_{1,2}$, which are introduced through $K_{jj'}$ from Eq. (10)] and the spontaneous emission frequencies which are determined by Eq. (12). We suppose here that $d_n \ll d_w$ and the narrow QW may be taken into account through the boundary condition

$$\left.\frac{d\phi_z}{dz}\right|_{-d_n/2}^{d_n/2} = U_0 \frac{2md_n}{\hbar^2}\phi_{z=0}, \tag{A1}$$

where U_0 is the band offset between narrow and wide QW's. Describing the first subband in the shallow level approximation we obtain

$$|\Delta\varepsilon_1| \simeq \frac{m_z}{(\hbar/d_n)^2}\frac{U_0^2}{2}, \quad \phi_{1z} \simeq \sqrt{\kappa}e^{-\kappa|z|}, \tag{A2}$$

where $\hbar\kappa = \sqrt{2m|\Delta\varepsilon_1|}$, $2/\kappa$ is the characteristic size of the first subband wave function. Since the orbital for the second subband is odd, then $\phi_{2z=0}=0$ and the boundary condition of Eq. (A1) is not essential for the second level description. Using the hard wall approximation at $z=\pm d_w/2$ we obtain simple expressions for the second subband:

$$\phi_{2z} \simeq \sqrt{2/d_w}\sin\frac{2\pi z}{d_w}, \quad \Delta\varepsilon_2 \simeq \frac{(2\pi\hbar/d_w)^2}{2m}. \tag{A3}$$

After the straightforward calculations of the integrals in Eq. (10) we obtain the simple expressions for the coefficients $k_{1,2}$:

$$k_1 \simeq \frac{2(2\pi)^2}{(\kappa d_w)^3}, \quad k_2 \simeq \frac{2}{3}\left(\frac{2\pi}{\kappa d_w}\right)^2. \tag{A4}$$

Analogous calculations give us the characteristic energy terms in the form

$$E_1^2 \simeq (2s\hbar\kappa)^2, \quad E_2^2 \simeq \frac{4}{3}\left(2\pi s\frac{\hbar}{d_w}\right)^2. \tag{A5}$$

We turn next to consider the LO-phonon emission frequencies given by Eq. (12), which are expressed through the factor

$$\sum_{j'\mathbf{p}'} |C_Q^{(LO)}|^2 \delta(E-\varepsilon_{p'}) = \frac{\alpha\hbar\omega_{LO}}{4\pi}\frac{\hbar}{L}\sqrt{\frac{2\hbar\omega_{LO}/m}{[\varepsilon+E+(\hbar q)^2/2m]^2-4\varepsilon E}}. \tag{A6}$$

Here α is the polaron coupling constant. We have performed the integration over 2D momenta using a δ function and taking a simple integral over the angular variable. Result for Eq. (12) is transformed into

$$\nu^{\pm}_{jj'}(\varepsilon)=\frac{\alpha\hbar\omega_{LO}}{2L}\sum_{q}\sqrt{\frac{2\hbar\omega_{LO}/m}{[2\varepsilon+\varepsilon_{jj'}\pm\hbar\omega_{LO}+(\hbar q)^2/2m]^2+4\varepsilon(\varepsilon+\varepsilon_{jj'}-\hbar\omega_{LO})}}|\langle j|e^{-iqz}|j'\rangle|^2. \tag{A7}$$

Thus the frequencies for transitions between the first subband states take the form

$$\nu^{+}_{11}(0)=\nu^{-}_{11}(\hbar\omega_{LO})=\alpha\hbar\omega_{LO}\int\frac{dq}{4\pi}\frac{\sqrt{2\hbar\omega_{LO}/m}}{\hbar\omega_{LO}+(\hbar q)^2/2m}|\langle 1|e^{-iqz}|1\rangle|^2, \tag{A8}$$

while the spontaneous emission from the second to the first subband is given by

$$\nu^{+}_{12}(0)=\nu^{-}_{21}(\varepsilon_0)=\alpha\hbar\omega_{LO}\int\frac{dq}{4\pi}\frac{\sqrt{2\hbar\omega_{LO}/m}}{\hbar\omega_{LO}+(\hbar q)^2/2m}|\langle 1|e^{-iqz}|2\rangle|^2. \tag{A9}$$

The integrals in Eqs. (A8) and (A9), as well as the characteristic intersubband velocity, $v_{\perp}=\langle 1|\hat{v}_z|2\rangle$, are evaluated in a straightforward manner by using the wave functions of Eqs. (A2) and (A3).

*Electronic address: ajhernan@ull.es
†Electronic address: fvasko@nmrc.ucc.ie

[1] B. K. Ridley, Rep. Prog. Phys. **54**, 169 (1991); P. J. Price, J. Appl. Phys. **53**, 6863 (1982).
[2] K. Yokoyama and K. Hess, Phys. Rev. B **33**, 5595 (1986); S. M. Goodnick and P. Lugli, *ibid.* **37**, 2578 (1988).
[3] C. Y. Sung, T. B. Norris, A. Afzali-Kushaa, and G. I. Haddad, Appl. Phys. Lett. **68**, 435 (1996); H. X. Li, Z. G. Wang, J. B. Liang, B. Xu, J. Wu, Q. Gong, C. Jiang, F. Q. Liu, and W. Zhou, J. Appl. Phys. **82**, 6107 (1997).
[4] J. F. Zhang and B. Y. Gu, Phys. Rev. B **43**, 5028 (1991); C. C. Yang, K. C. Huang, and Y. K.Su, Jpn. J. Appl. Phys., Part 2 **35**, L535 (1996).
[5] S. I. Borenstain and J. Katz, Appl. Phys. Lett. **55**, 654 (1989); A. Kastalsky and V. J. Goldman, *ibid.* **59**, 2636 (1991); A. N. Korotkov, D. V. Averin, and K. K. Likharev, *ibid.* **65**, 1865 (1994); F. T. Vasko and Yu. N. Soldatenko, *ibid.* **66**, 544 (1995).
[6] M. Helm, Semicond. Semimetals **62**, 1 (2000).
[7] C. Gmachl, F. Capasso, D. L. Sivco,and A. Y. Cho, Rep. Prog. Phys. **64**, 1533 (2001).
[8] R. Kohler, A. Tredicucci, F. Beltram, H. E. Beere, E. H. Linfield, A. G. Davies, D. A. Ritchie, R. C. Iotti, and F. Rossi, Nature (London) **417**, 156 (2002).
[9] J. Ulrich, R. Zobl, W. Schrenk, G. Strasser, K. Unterrainer, and E. Gornik, Appl. Phys. Lett. **77**, 1928 (1995); J. Ulrich, R. Zobl, N. Finger, K. Unterrainer, G. Strasser, and E. Gornik, Physica B **272**, 216 (1999).
[10] R. Colombelli, A. Straub, F. Capasso, C. Gmachl, M. I. Blakey, A. M. Sergent, S. N. G. Chu, K. W. West, and L. N. Pfeiffer, J. Appl. Phys. **91**, 3526 (2002); R. Kohler, A. Tredicucci, E. Beltram, H. E. Beere, E. H. Linfield, A. G. Davies, and D. A. Ritchie, Appl. Phys. Lett. **80**, 1867 (2002).
[11] Under the condition $\varepsilon_2 \ll \varepsilon_{21}$ one can consider the system (28) with the energy fluxes given by Eqs. (29) and (13) as a simplified system with constant coefficients. The general solution for such a system is a linear combination of the fundamental solutions $\exp(x\varepsilon/T)$ with the roots x determined from the third-order characteristic equation. The coefficients in such linear form are determined from the boundary conditions in Eq. (32) and the normalization condition in Eq. (17).
[12] W. H. Press, S. A. Teukolsky, W. T. Vetterling, and B. P. Flannery, *Numerical Recipes in Fortran 77. The Art of Scientific Computing* (Cambridge University Press, Cambridge, England, 1999).
[13] F. T. Vasko and A. Kuznetsov, *Electronic States and Optical Transitions in Semiconductor Heterostructures* (Springer, New York, 1998).
[14] P. Hyldgaard and J. W. Wilkins, Phys. Rev. B **53**, 6889 (1996); M. Hartig, J. D. Ganire, P. E. Selbmann, B. Deveaud, and L. Rota, *ibid.* **60**, 1500 (1999); K. Kempa, P. Bakshi, J. Engelbrecht, and Y. Zhou, *ibid.* **61**, 11 083 (2000).
[15] F. T. Vasko and E. P. O'Reilly, Proceedings of the 26th International Conference on the Physics of Semiconductors, Edinburgh, 2002.
[16] P. Kinsler, R. M. Kelsall, and P. Harrison, Physica B **263**, 507 (1999).
[17] H. Haken, *Synergetics* (Springer, Berlin, 1983); E. Scholl, *Nonequilibrium Phase Transitions in Semiconductors* (Springer, Berlin, 1987).